Check for updates

Enhanced crystallisation kinetics of edible lipids through the action of a bifurcated streamer†

Jack J. Youngs, [a] Peter R. Birkin, *[a] Juhee Lee,[b] Tadd T. Truscott [c] and Silvana Martini [b]

The processing of healthy foods remains a challenge and any technology with the ability to tailor the physical properties of new materials is in demand. High-intensity ultrasound (HIU) has been identified as a useful processing technique for such activities particularly for edible lipids. HIU has been known to alter the crystallisation kinetics and in turn the resultant physicochemical properties for specific food applications. The role of cavitation dynamics during treatment of oils with HIU is of interest, with the knowledge gained allowing for insight into the complex and still undefined mechanism of action. To this end, the crystallisation kinetics of an edible lipid were investigated in the presence of several distinctly different cavitation conditions. Several cavitation clusters, including a bifurcated streamer (BiS), located on the surface of a piston-like emitter (PLE) were studied, each generated by a specific ultrasonic power level. Only samples crystallised at a low supercooling (ΔT_{SC}) value display significant differences in induction time for each of the selected HIU powers, at least 5 minutes earlier than without exposure to HIU. Substantially better energy efficiencies were seen for the BiS regime (ΔT_{SC} = 5 °C) which coincided with maximal crystal growth rates. An increase in melting enthalpy and elastic modulus is reported in the presence of HIU for all crystallisation temperatures, this effect is larger overall with increasing ultrasonic power. In addition, sonicated samples in the presence of the BiS event were composed of fewer smaller crystals compared to higher HIU powers after 60 minutes at 30 °C. Bubble dynamics recorded during a 10 s sonication period exhibited a greater acoustic attenuation effect for the highest ultrasonic power (75 W). The results suggest that the dynamics of the cluster and the presence of the BiS event are important in terms of energy efficiency and the physical properties of the crystallised lipid material.

Introduction

Gas bubbles, and cavitation, can play an important role in a number of processes and applications.[1–3] To maximise the efficiency of these systems, a thorough understanding of the processes involved, and the mechanisms associated with them, is crucial. Cavitation is commonly generated by the application of high-intensity ultrasound (HIU) within liquids, driven by the interaction between pressure variations (*e.g.* ultrasonic waves) and pre-existing gas bubbles/bubble nuclei.[4,5] Such environments can be highly dynamic, with gas bubbles rapidly growing/collapsing, fragmenting and coales-

cing with one another. The relative size of the gas bubbles, their motion and life-cycle are termed cavitation or bubble dynamics and can result in extreme localised conditions, with temperatures of approximately 5000 K and local pressures of ~1–10 kbar generated.[6,7] Cavitation, within aqueous media, has been extensively studied and, while there are reports of its effects in non-aqueous and non-Newtonian fluids, studies in edible lipids require considerably more attention. The importance of these materials is clear, with the estimated global edible oils and fats market forecast to show compound annual growth rates (CAGR) of 7.1%, with a net worth of approximately $165 billion by 2026.[8]

HIU has been employed as an effective processing tool to enhance the crystallization behaviour of healthier edible lipid systems, through inducing the onset of crystallisation and altering their physicochemical properties.[9–12] Edible lipids deliver the desirable nutritional and functional attributes of many food products, which play a large role in consumer acceptance and the overall food quality.[13,14] The chemical composition of lipids, such as the fatty acid length and degree of saturation, is critical. In general, lipids that contain long

a Department of Chemistry, University of Southampton, Southampton, SO17 1BJ, UK. E-mail: prb2@soton.ac.uk
b Department of Nutrition, Dietetics, and Food Sciences, Utah State University, Logan, UT, 84322-8700, USA
c Department of Mechanical and Aerospace Engineering, Utah State University, Logan, UT, 84322-4130, USA
† Electronic supplementary information (ESI) available. See DOI: 10.1039/d1an00437a

chain saturated fatty acids and partially hydrogenated oils (PHOs) display greater sample texture and elasticity compared to liquid oils with lower levels of saturated fatty acids or with shorter chain lengths. The use of PHOs has been strongly linked to cardiovascular disease due to high levels of trans-fats and, since June 2015, no longer hold the 'Generally Recognised as Safe' (GRAS[15]) status.[16–18] This presents a clear challenge within the food industry, with healthier trans-fat free alternatives lacking specific physical structure and predominantly existing as liquid oils.

Previous reports have demonstrated that HIU can improve the nucleation kinetics of the lipid crystallisation process,[19–22] which give crystalline networks formed of a greater number of smaller diameter crystals. Greater lipid supercooling has been shown to give similar results. However, the crystal framework is less stable with imperfections compared to reduced supercooling conditions.[23–26] The degree of supercooling and the applied ultrasonic power can have a significant impact upon the nature of the cavitation events that occur within these complex lipid systems.[27–30] In particular, the dynamics of the cavitation cluster produced directly beneath the HIU source and the existence of a bifurcated streamer (BiS) system, are of significant interest.[31] The exact physical mechanism responsible for the action of HIU within edible lipids is currently unclear, which limits the exploitation of this novel processing technique. The study of such gas bubble events has potential to rationalise the diverse crystallisation behaviour observed within sonicated lipids and provide an opportunity to tailor their physical characteristics. Many studies have investigated the effect of ultrasonic power level upon lipid crystallisation behaviour.[19,32–35] However, selecting the conditions based on the observed cluster dynamics has received little attention. This is particularly true for the unusual BiS event, as this appears as a rather unusual phenomena at this time, present in oils.

The aim of the work presented here was to evaluate the changes in the crystallisation kinetics and physical characteristics of an all-purpose shortening material in response to selected HIU conditions. In the conditions selected, the bubble dynamics produced within the sample during the initial critical crystallisation stages were fixed to different cluster types including the bifurcated streamer system. This selection was achieved by controlling the applied ultrasonic power (and consequantly the amplitude of oscillation of the piston like emitter, PLE, tip). Lastly, the effect of the supercooling conditions upon crystallisation kinetics and resultant materials were also analysed. Each of the ultrasonic powers explored in this study was associated with a distinct cavitation cluster event previously observed within a liquid soybean oil sample.[28,36]

Methods

Materials

Commercial all-purpose shortening (APS, Bunge) was crystallised at temperatures of 26 °C and 30 °C with and without the application of high-intensity ultrasound (HIU) at several ultrasonic powers. The melting point of the sample was 35.1 ± 0.4 °C and was determined using AOCS Official Method Cc 1–25.

Crystallisation and ultrasound application

Samples were melted in a microwave oven and then stored in an oven at 80 °C for 30 minutes to remove residual crystal memory. The melted sample (100 g) was transferred to a double-walled thermostatic crystallisation cell connected to an external water bath (Grant, LT ecocool 100), set to the particular crystallisation temperature (T_c) used in this study. The degree of super cooling (ΔT_{SC}) is defined as ($T_m - T_c$) where T_m the melting point of the sample. A schematic of the experimental set-up is detailed in Fig. 1. Two temperatures were selected to represent conditions where HIU has a prominent effect upon the physical properties of the fat (T_c = 30 °C) in addition to such conditions where HIU may have a less significant effect (T_c = 26 °C).[12] The sample was agitated using a magnetic stirrer (200 rpm) to enhance heat transfer between the sample and the circulating water. Agitation was conducted for approximately 6 and 10 minutes for T_c = 26 °C and 30 °C respectively. The APS sample was crystallised in both the absence and the presence of ultrasonic stimuli. HIU was delivered using a Misonix S-3000 sonicator (Misonix Inc., Farmingdale, New York, USA) operating at an acoustic frequency of 20 kHz. The tip or piston-like emitter (PLE) of this device (3.2 mm diameter) was driven at five ultrasonic powers (10 W, 18 W, 36 W, 51 W and 75 W) each selected to stimulate different cluster conditions for a duration of 10 s. These powers were selected by observing the acoustic emission corresponding to the appropriate cluster.[37]

Each cluster undergoes a repetitive growth-collapse phase with a lower frequency relative to the frequency of the HIU
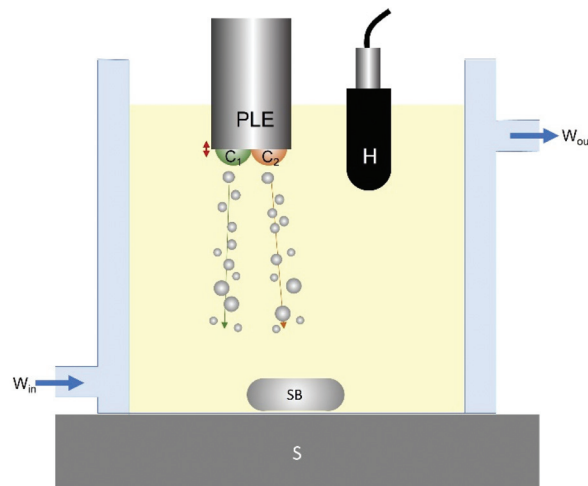

Fig. 1 Schematic representation of the experimental setup used for the crystallisation experiments. Here a BiS event is represented by two clusters (C$_1$ and C$_2$) generated at the PLE tip with two streams of bubbles (labelled with arrows). A hydrophone (H) and stirrer(S)/stirrer bar (SB) are included. The temperature of the system is controlled through the water jacket with the flow direction indicated. Not to scale.

Table 1 Bubble cluster collapse frequency (f/n) for each of selected HIU power levels, where f is the HIU drive frequency and 'n' is an integer value. Four single bubble clusters (18 W, 36 W, 51 W and 75 W) and one bi-cluster (or bifurcated streamer, BiS, at 10 W) are shown. Within the bi-cluster regime, the collapse of the first cluster is 180° out of phase of the second, each operating at $f/2$ collapse frequency. Hence, a cluster collapse occurs every cycle of the sound source in this case*

Power/W	10	18	36	51	75
Bubble cluster and collapse frequency	$f/2 + f/2'$ (10 kHz, 20 kHz*)	(5 kHz)	$f/5$ (4 kHz)	$f/6$ (3.3 kHz)	$f/7$ (2.9 kHz)

source. The bubble cluster collapse frequency is given by f/n where f is the frequency of the HIU source and n is an integer value. Table 1 summarises the HIU power levels selected to deliver each distinct bubble cluster type.

The PLE tip was positioned approximately central (x–y direction) within the cell. Previous research has identified that ultrasonic stimuli have a greater effect on the induction time of lipid crystallisation in the presence of crystals.[12,20] Therefore, HIU was applied at the onset of crystallisation, as indicated by a slight increase in sample turbidity. This correlated to times of 11 minutes and 16 minutes for T_c = 26 and 30 °C, respectively. The crystallisation behaviour of the samples was monitored as a function of time for a total 60 minutes after initial cooling (see Fig. S1 (ESI†)).

Melting behaviour

A differential scanning calorimeter (DSC-TA Instruments, New Castle, DE, USA) was employed to measure the melting behaviour of the crystallised lipid sample. The sample material (5–15 mg) was transferred to a hermetic aluminium pan, sealed with a lid, and then transferred to the DSC oven stabilised at the relevant T_c (26 °C or 30 °C). This represents a supercooling condition of ΔT_{SC} = 9 °C and 5 °C respectively. Samples were maintained at this temperature for 1 minutes and then heated from T_c to 80 °C at 5 °C per minute. The peak melting temperature (T_p) and melting enthalpy (ΔH_m) were recorded. Heat flow measured as a function of temperature *vs.* empty reference pan.

Crystal microstructure

A polarised light microscope (PLM-Olympus BX 41, Tokyo, Japan) fitted with a digital camera (Infinity 2, Lumenera Scientific, Ottawa, Canada) was used to record the crystal microstructure of crystallised lipid material. Images were recorded before and after application of HIU at approximately 6, 10, 18 and 60 minutes after initial sample cooling.

Viscoelastic properties

A magnetic bearing rheometer (model AR-G2, TA Instruments, New Castle, DE, USA) was used to measure the elasticity of crystallised samples after approximately 60 minutes of crystallisation. A parallel plate geometry (40 mm diameter) was employed and maintained at the relevant T_c (26 °C or 30 °C). Depending upon the relative hardness of the sample, a gap of

between 500–1000 μm was used. Oscillatory tests were performed by a strain sweep step from 0.0008–10% of strain and equilibration time of 1 minute. Viscoelastic parameters such as the storage modulus (G') were recorded at 0.01% of strain.

Hardness

The hardness of the crystallised material was evaluated by texture profile analysis (TPA) using a Texture Analyser (model TA, XT Plus, Texture Technologies Corp., Scarsdale, NY, USA). Samples were transferred to labelled plastic tubes (1 cm diameter) after 60 minutes and stored at 5 °C for 48 h. Note this is a common technique used in the evaluation of physical properties of fats. Even though the conditions under which hardness was measured are different from the others (*e.g.*, 5 °C *vs.* 25 °C) the results still give valuable information about the physical properties of the crystalline network. Chilled samples were cut to a height of approximately 1 cm, placed on the sample platform and a two-step compression with 5 cm diameter cylindrical probe was performed. A constant speed of 5 mm s⁻¹ and compression strain of 25% were employed. Data was not recorded at 60 minutes after processing as the lipid sample was too soft to measure hardness at this time.

Cavitation

The cavitation dynamics present within the APS sample were evaluated using a hydrophone (Reson, TC4013), positioned approximately 20 mm to the side of the PLE tip. An oscilloscope (Owon DS7102V) was employed to visualise and capture the hydrophone signal over the first 1000 ms of PLE tip operation. The acoustic emission was also recorded over a total 15 s period, featuring the first 10 s of the applied HIU pulse plus an additional 5 s in the absence of HIU. The data in this period was captured using an in-house generated program (Visual Studio 2010, Measurement Studio 2012) and a USB-204 DAQ card (Measurement Computing). The data acquisition regime is detailed in Fig. S1.†

Measurement of solid fat content (SFC)

Samples remained within the crystallisation cell until the application of high intensity ultrasound (HIU) had been completed. They were then transferred to p-NMR tubes, previously preheated to the crystallisation temperature (T_c). The p-NMR tubes were placed in a water bath set at the relevant temperature (T_c). The crystallisation behaviour of the samples was then monitored by recording the SFC *vs.* time using NMR Minispec mq20 series (Bruker, California, USA). The SFC was measured immediately after the sample was removed from the crystallisation cell and every 1 minute until the end of crystallisation (60 minutes). Note, SFC values prior to HIU treatment are assumed to be zero. This assumption is supported by the woHIU measurements.

Crystallisation kinetics

The SFC *vs.* time data were fitted to the reparametrized Gompertz equation[38] (eqn (1)).

$$\text{SFC}_t = \text{SFC}_m e^{-e\left[\left(\frac{2.718\mu(\lambda-t)}{\text{SFC}_m}\right) + 1\right]} \qquad (1)$$

where SFC_t is the solid fat content measured at time, t, SFC_m is the final solid fat content, μ is the maximal growth rate here quoted in % min^{-1} and λ is the induction time of crystallisation (min). This equation has been used previously to describe isothermal crystallisation of fats.[26,38,39]

Statistical analysis

Crystallisation experiments were performed in triplicate and physical properties were measured in triplicate (SFC and microstructure) and duplicate (DSC and elasticity). Significant differences (α = 0.05) were evaluated by two-way ANOVA using GraphPad Prism software (version 8.21 for Windows, San Diego, CA, USA). Table 2, and some figures, show which data is insignificantly different to one another by assignment of the same symbol annotation. For example, if the annotation changes (*e.g.*, from 'a' to 'b' or 'α' to 'β'), there is a significant difference between those measurements under the conditions stated. In the tables and plots, data associated with experiments at 26 °C are annotated with 'a, b' *etc.* while those at 30 °C are annotated with 'α, β' *etc.*

Results and discussion

Solid fat content

Fig. 2 depicts the crystallisation behaviour of an all-purpose shortening (APS) sample, analysed by following the solid fat content (SFC) *vs.* time profile. Here a series of different acoustic power levels were employed under two supercooling conditions of ΔT_{SC} = 9 °C (Fig. 2A, 26 °C) and ΔT_{SC} = 5 °C (Fig. 2B, 30 °C). APS samples were also crystallised in the absence of HIU (●) and were analysed for comparison under identical conditions. SFC values were fitted to the Gompertz model and all samples exhibited r^2 values greater than 0.94. Gompertz fitting parameters including the maximum solid fat content after 60 minutes of crystallisation (SFC_m), the maximal crystal growth rate (μ) and the induction time for lipid crystallisation (λ) are summarised in Table 2. Fig. 2A shows the SFC curves for sonicated and non-sonicated APS samples crystallised at T_c = 26 °C (ΔT_{SC} = 9 °C), where the sample was exposed to HIU at 11 minutes as indicated by the vertical dashed line (---) and the arrow.
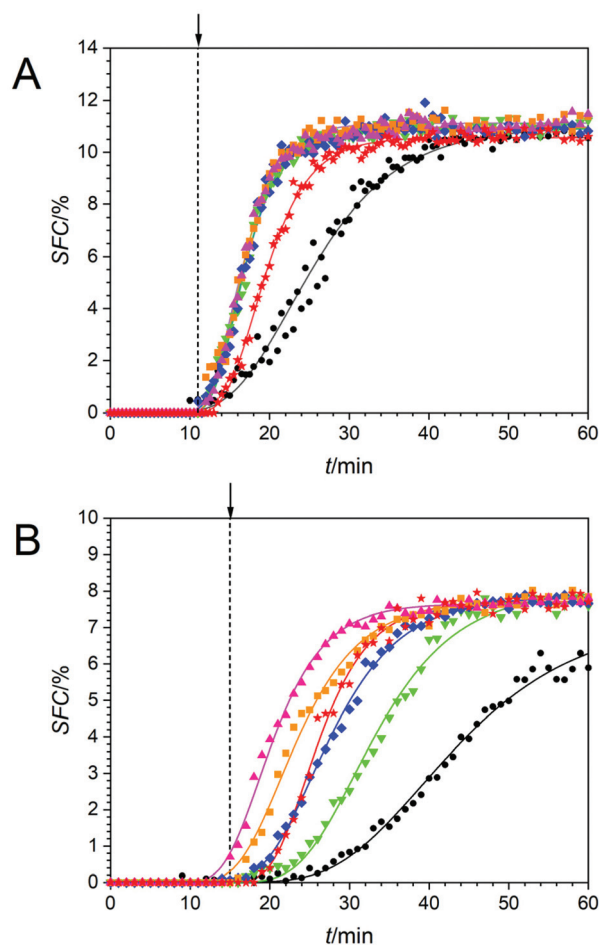

Fig. 2 SFC of all-purpose shortening (APS) during 60 minutes of crystallisation at 26 °C (A) and 30 °C (B) in the absence (•) and presence of high-intensity ultrasound (HIU) operating at 10 W (★), 18 W (▼), 36 W (◆), 51 W (■) and 75 W (▲). The dotted vertical line, (---), and arrow indicated the time when HIU was applied to the system.

At T_c = 26 °C the SFC of all samples increased over time in a sigmoidal like manner reaching a plateau value at an average of ~11%. However, the time needed to reach the plateau was found to be the same for all HIU treated samples

Table 2 Kinetic parameters obtained from the Gompertz model from the isothermal crystallisation of APS without and with HIU at power levels between (0–75) W, each power corresponding to a different cavitation cluster system. Data shown as a mean with 95%CL in parenthesis. For each of the kinetic parameters, data with different superscripts are statistically different (p = 0.0001) compared to each other within the respective column. A change in superscripts indicate whether these figures are significantly different to one another (read in the columns). Note 'a, b' *etc.* corresponds to ΔT_{SC} = 9 °C with 'α, β' *etc.* correspond to ΔT_{SC} = 5 °C

W	ΔT_{SC} = 9 °C			ΔT_{SC} = 5 °C		
	SFC_m/%	μ/% min^{-1}	λ/min	SFC_m/%	μ/% min^{-1}	λ/min
0	10.9[a] (0.1)	0.6[a] (0.1)	17[a] (1)	7.3[α] (0.2)	0.29[α] (0.04)	29[α] (1)
10	10.6[a] (0.1)	1.1[b] (0.2)	14.4[b] (0.3)	7.7[α,β] (0.2)	0.7[β,χ] (0.1)	20.1[β] (0.4)
18	11.0[a] (0.1)	1.3[b] (0.1)	12.5[c] (0.2)	8.0[β] (0.1)	0.42[δ] (0.04)	23.7[χ] (0.2)
36	10.8[a] (0.4)	1.4[b] (0.4)	13.0[b,c] (0.3)	7.9[β] (0.1)	0.48[χ,δ] (0.06)	19.2[δ] (0.2)
51	11.1[a] (0.06)	1.3[b] (0.1)	12.3[c] (0.5)	7.7[α,β] (0.2)	0.53[χ] (0.03)	16.0[ε] (0.9)
75	10.8[a] (0.4)	1.4[b] (0.1)	12.7[b,c] (0.1)	7.7[α,β] (0.3)	0.63[β] (0.02)	14.2[φ] (0.6)

(~25 minutes) except for the BiS event, which took ~35 minutes. This limiting consistent rate is attributed to a rate limiting process associated with the crystallisation of the APS sample under these conditions. In the absence of HIU treatment, the time to reach the plateau was greater still at ~45 minutes.

Fig. 2B shows the SFC curves for sonicated and non-sonicated APS samples crystallised at T_c = 30 °C (ΔT_{SC} = 5 °C), where HIU was applied at 15 minutes as indicated (---). Note this delayed application time is a consequence of the reduced supercooling applied to the samples in this data set. In addition, although the predicted induction time can be estimated to be less than the application time for HIU, this is an artefact of the analysis method used. Here the fit predicts the λ value. This is apparent by looking at the data prior to the HIU application where all the SFC's are essentially zero. After the HIU has been applied there is a clear jump in the data (see 75 W, ΔT_{SC} = 5 °C for example) which when the fit is applied, yields a λ value of 14.2 min which is below the HIU application time.

The SFC of all sonicated samples increased over time and reached a plateau value after progressively shorter times when conventional clusters were considered (for 18 W, 36 W, 51 W and 75 W). While the BiS event, with its bi-cluster cavitation environment,[31] which although observed at the lowest applied power of 10 W (★), reaches a plateau at an intermediate time point within the data set of ~40 minutes. The evidence suggests that the BiS cluster is more efficient when compared to clusters at 18 W and 36 W (even though only 10 W is used to generate the BiS event under these conditions). APS samples crystallised in the absence of HIU reached a plateau SFC value after approximately 60 minutes, which indicates that sonication at lower supercooling (e.g., ΔT_{SC} = 5 °C vs. ΔT_{SC} = 9 °C, see Fig. 2) also promotes lipid crystallisation as expected.[10,25] The actual SFC_m values are displayed in Table 2. The SFC_m values were found to be similar for a particular supercooling regime. This is attributed to the SFC_m value not being dependent upon the kinetics of crystallisation under each treatment, but rather the composition of the triacylglycerol (TAG) components[40] within the lipid sample, and the proportion of TAG's that crystallise under the selected conditions. In all cases, however, the final SFC_m values were significantly lower at 30 °C compared to 26 °C, likely as a result of a greater thermodynamic driving force for crystallisation[26] at the lower temperature and hence higher supercooling value.

Non-sonicated APS samples had significantly longer induction times (λ) for crystallisation and slower crystal growth rates (μ) when compared to those treated with HIU. Note, to further highlight the effect of HIU on these systems, changes in these parameters with respect to the non-sonicated sample at each of the ultrasonic powers deployed (for example $\Delta\lambda$ and $\Delta\mu$) were calculated (see Table S1†).

Fig. 3A shows the $\Delta\lambda$ values at T_c = 26 °C ($\diamond$) and 30 °C ($\blacklozenge$). The values of $\Delta\lambda$ were not significantly different for samples treated at all HIU powers at 26 °C. Fig. 3A shows that a greater variation in induction times for crystallisation were observed for different HIU powers applied at 30 °C. This suggests that

the nature of the HIU treatment is more critical under lower supercooling (ΔT_{SC} = 5 °C) conditions.[10,23] In general, the value of $\Delta\lambda$ increased with HIU power for samples crystallized at 30 °C. However, an unusually high $\Delta\lambda$ value compared to all higher HIU powers (p = 0.001) was seen for the bifurcated streamer (10 W) case in agreement with the results shown in Fig. 2B. Fig. 3B depicts values of $\Delta\lambda$ per watt of power applied to the oil sample for each of the crystallisation conditions. At 26 °C, values were similar for all HIU. In contrast, treatment of the APS sample at 30 °C with the bifurcated streamer (10 W) showed a notably enhanced energy efficiency compared to all other conditions (p < 0.05). The exact nature of the greater effect the BiS event has on the crystallisation process, compared to a single cluster, remains to be ascertained. However, the BiS event, has two streamers and a pair of clusters. This will expose the fluid to relatively more collapses per cycle of the PLE (compared to $f/3$ say) and possibly a greater number of active bubbles in the dual streamers. These combined characteristics could enhance the kinetics through greater secondary crystal nucleation, for example.

Fig. 3C illustrates the change in maximal crystal growth rate ($\Delta\mu$) for each of the HIU treatments relative to the woHIU case. No significant changes in crystal growth rates are observed at 26 °C (p < 0.1). However, Fig. 3C does show that significantly lower crystal growth rates observed at 30 °C compared to 26 °C for all applied acoustic powers. Values of μ at 30 °C increased as HIU power levels rose from 18 W. Note that the presence of the BiS event (10 W) exhibited a greater than expected crystal growth rate (p = 0.001) and was, significantly higher than 18 W power. It was found to be comparable to more energy intensive treatments of 75 W (p > 0.1) at 30 °C (see Table 2). Fig. 3D emphasises this point as the greatest crystal growth per watt of power was seen for 10 W for both 26 °C and 30 °C. This effect was most prominent at 30 °C, with significant difference in values compared to all other HIU powers (p < 0.05). In addition, the $\Delta\mu$ value was independent of crystallisation temperature, for the two temperatures studied, in the presence of the BiS environment (10 W).

Crystal microstructure

Fig. 4 shows polarised light microscopy (PLM) images of APS samples crystallised in the presence and absence of HIU at 26 °C and 30 °C recorded after 60 minutes. Images recorded without (woHIU) HIU at 26 °C show the presence of a large number of small lipid crystals and demonstrate clear differences from the sample crystallised at 30 °C (woHIU), which depicts a more open crystal network with considerably fewer lipid crystals of larger diameter. Larger crystals are expected in samples crystallized at higher temperature due to the lower supercooling.[10,26] Qualitatively, sonicated samples crystallised at 26 °C display only minor changes in the crystal microstructure, with a slightly more open framework for the 10 W treatment compared to higher acoustic powers (image rows 3–6). In contrast, the influence of HIU upon crystal size after 60 minutes is greatest for T_c = 30 °C, where even the application of low powers (e.g., the BiS event at 10 W) results in a
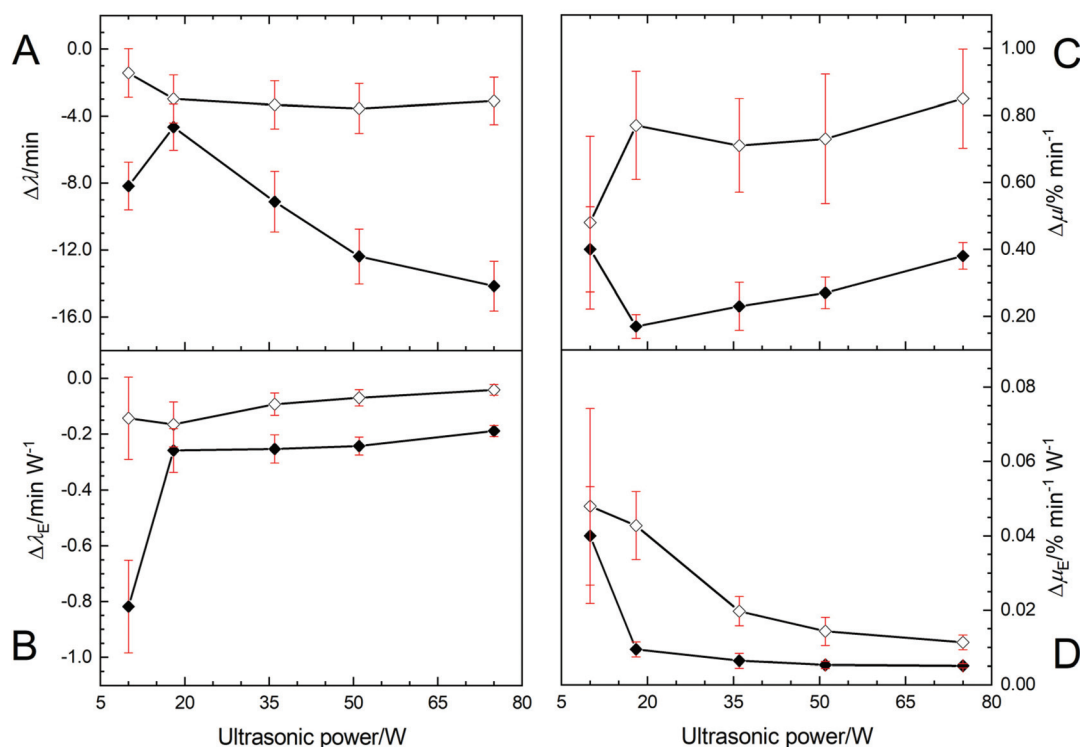
Fig. 3 Plot showing the change in induction time of crystallisation ($\Delta\lambda$) (A) and change in induction time per watt of ultrasonic power ($\Delta\lambda_E$) (B) for APS treated at 26 °C ($\diamond$) and 30 °C ($\blacklozenge$) as a function of HIU power. (C) Plot showing the change in maximal crystal growth rate ($\Delta\mu$) and (D) shows the change per watt of ultrasonic power ($\Delta\mu_E$) for APS treated at 26 °C ($\diamond$) and 30 °C ($\blacklozenge$) as a function of HIU power. Mean values are plotted with 95% confidence levels, recorded over three replicate crystallisation experiments. In each case, mean values were compared to those crystallised without HIU under identical supercooling conditions.

clear reduction in the diameter of lipid crystals present. Overall larger lipid crystal diameters were exhibited at this lower supercooling (ΔT_{SC} = 5 °C) condition, with crystal clusters of variable sizes observed for a HIU power of 18 W. Whereas only minor changes in the crystal microstructure are documented for (36–75) W with these sample displaying greater homogeneity in crystal size and shape. The images in Fig. 4 are consistent with the results discussed in the previous solid fat content section, where the presence of HIU, at all acoustic powers studied, alter the crystallisation process and lead to the formation of a more densely packed crystalline network. This is consistent with observations seen previously within different lipid media and provides evidence for a secondary nucleation effect that occurs as a consequence of enhanced crystal contact and shear[22,41,42] in the presence of HIU.

Hardness

Fig. 5 shows the hardness of APS crystallised for 60 minutes at 26 °C ($\square$) and 30 °C ($\blacksquare$), in the absence (woHIU) and presence of high-intensity ultrasound. In the absence of HIU, hardness (HA) values at each treatment condition were not significantly different for the two crystallisation temperatures employed. In general, the hardness of the crystal network increased with increasing acoustic power level between 10 W and 75 W and becomes statistically different (p = 0.002) compared to the

woHIU treatment above 18 W (see dotted vertical demarcation line). The value of sample hardness was independent of HIU power level above 18 W HIU power at both supercooling conditions. Note that during storage at 5 °C samples (which is the same for all samples) were exposed to very high supercooling (ΔT_{SC} ~30 °C), and any remaining liquid components crystallise rapidly. Changes in the sample hardness (ΔHA) relative to the woHIU treatment are given in Fig. S4(A)† and the changes per watt of power (ΔHA$_E$) are detailed within Fig. S4(B).† The change in sample hardness showed little difference between 26 °C and 30 °C temperatures over the HIU power level range. In addition, the change in hardness per watt were also rather insignificant. Mean values and 95% confidence intervals are summarised in Table S4 (ESI).†

Viscoelastic properties

Fig. 6 depicts the elastic modulus (G') of the APS samples crystallised for 60 minutes at 26 °C ($\square$) and 30 °C ($\blacksquare$). Samples crystallised in the absence of HIU showed significantly reduced values for G' compared to all sonicated samples (10 W–75 W) (p < 0.05) at 26 °C and between 36 W–75 W at 30 °C (p < 0.05). These low values of G' for the non-sonicated sample could be attributed to the crystal structure of the material. Fig. 4 showed that without HIU the sample contained fewer but larger crystals[43] which presumably give a less densely packed structure
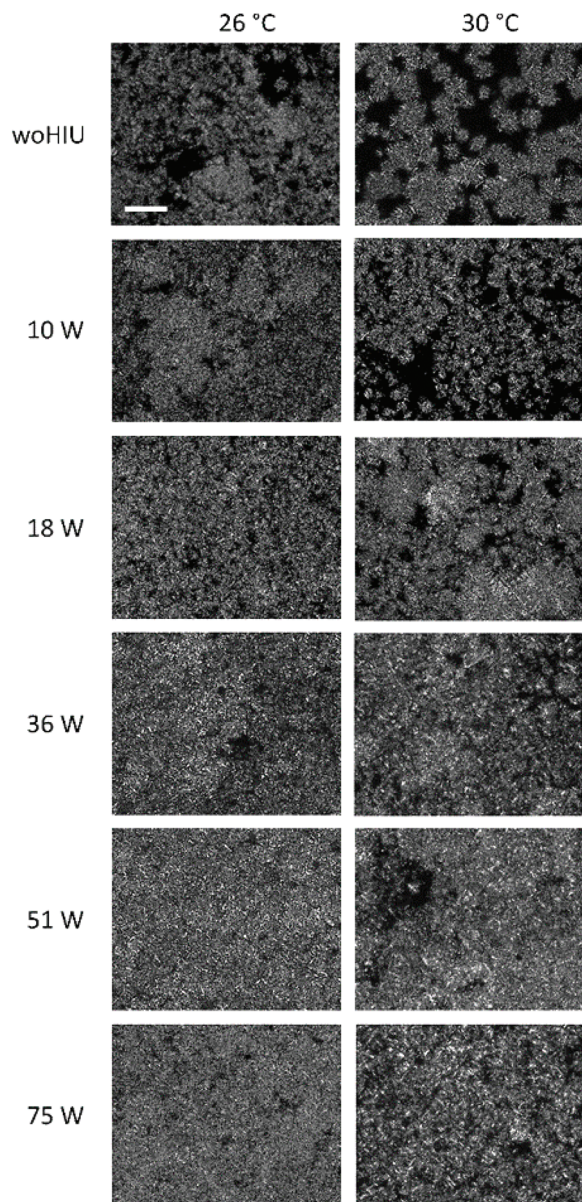
Fig. 4 Polarised-light microscopy (PLM) image panel of APS crystallised at T_c = 26 °C and 30 °C with and without (row 1) high-intensity ultrasound (HIU) pulse operating at 20 kHz frequency over 10 s period. HIU applied at power levels of (10, 18, 36, 51 and 75) W, depicted by images in rows 2–5 respectively. Images recorded after 60 minutes. Scale bar in *top left* image represents 100 μm.

Fig. 5 Plot showing the hardness (HA) of APS measured after storage at 5 °C for 48 h. Samples were crystallised for 60 minutes at 26 °C (☐) and 30 °C (▨) in the presence and absence (woHIU) or with different HIU power level. Hardness values become significantly different from the woHIU treatment for both temperatures above HIU power levels as indicated (−−). Mean hardness values are plotted with 95% confidence levels from twelve repeat measurements, recorded over three replicate crystallisation experiments.

Fig. 6 Plot showing the elastic modulus (G') of APS crystallised for 60 minutes at 26 °C (☐) and 30 °C (▨) in the presence and absence (woHIU) of HIU. G' values become significantly different from the woHIU treatment for all HIU power levels at 26 °C (as indicated (−−)) and above 10 W power for 30 °C (as indicated (−−)). Mean values are plotted with 95% confidence levels from nine repeat measurements, recorded over three replicate crystallisation experiments.

compared to sonicated APS samples. In all cases, the values were significantly different for the same HIU power at the two crystallisation temperatures employed. The changes in the elastic modulus (see Fig. 7A) becomes significantly different (p = 0.002) compared to the woHIU for all ultrasonic power levels at 26 °C but required powers greater than 18 W at 30 °C.

Although the effect of the BiS environment is prominent within the kinetics of crystallisation, its influence within the physical properties is less pronounced although these parameters appear less power dependant compared to other measurements.
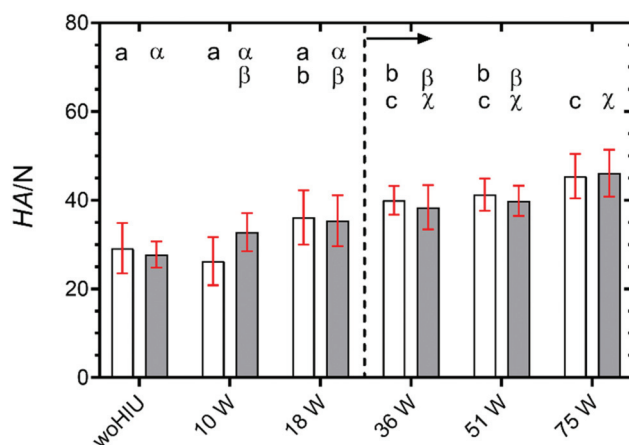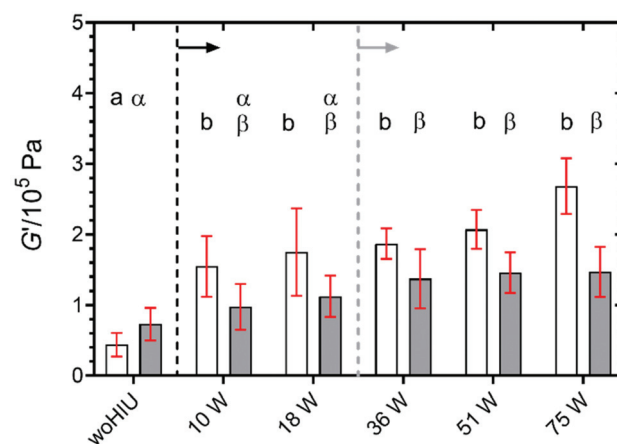
Fig. 7B shows the changes in elastic modulus per watt of HIU power ($\Delta G'_E$). The greatest values for this parameter were found at the lower power levels. At 10 W the difference in these values was significantly greater (p < 0.05) compared to samples sonicated above 18 W HIU power. Whereas G'_E values associated with all other HIU treatment and temperature conditions were statistically non-significant (p > 0.2). The viscous modulus (G'') of the APS samples was also determined with and without HIU treatment at selected power levels between 10 W–75 W (see Fig. S2 (ESI)†). At high supercooling (ΔT_{SC} = 9 °C)
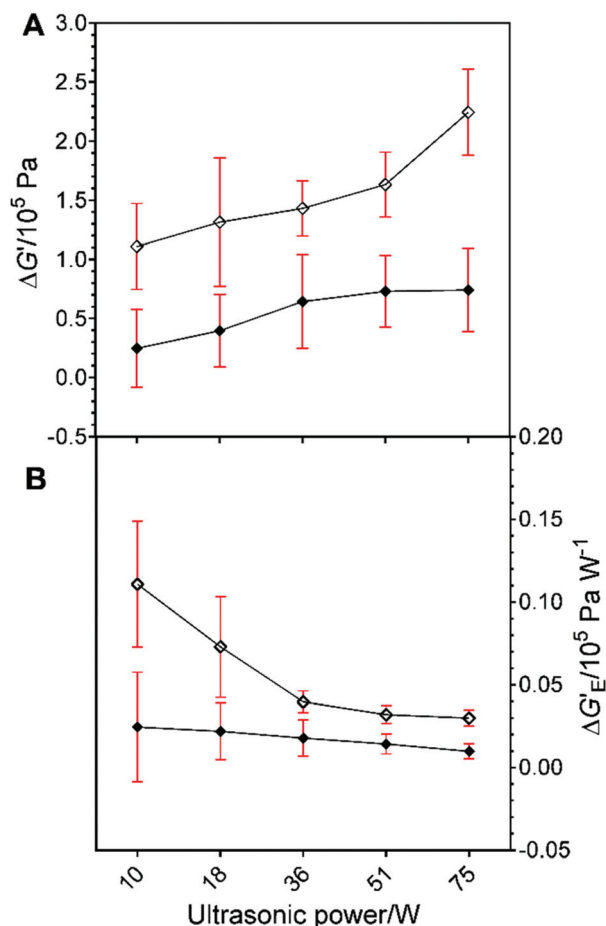
Fig. 7 Change in elastic modulus ($\Delta G'$) (A) relative to woHIU treatment and change per W ($\Delta G'_E$) (B) from the isothermal crystallisation of all-purpose shortening in the presence of HIU, delivered at selected powers between (10–75) W with respect to untreated (woHIU) samples, at T_c = 26 °C ($\diamond$) and 30 °C ($\blacklozenge$). Mean values are plotted with 95% CL.

the values of G'' increased for sonicated samples compared to woHIU treatments, except in the presence of the BiS environment (10 W) where a small decrease was reported. The differences in G'' were only significant from samples in the absence of HIU above 36 W applied power. As such, the viscous modulus was not statistically different for samples without HIU and those sonicated at 10 W or 18 W powers. At lower supercooling (ΔT_{SC} = 5 °C), all sonicated samples except that treated at 10 W showed increases values of G'' compared to in the absence of HIU. In addition, changes in viscous modulus ($\Delta G''$) (see Fig. S4 (C) (ESI)†) and changes per watt of HIU power ($\Delta G''_E$) (see Fig. S4 (D) (ESI)†) were recorded. Values of $\Delta G''$ were independent of crystallisation temperature for all HIU power levels except 18 W, which showed the greatest energy efficiency ($\Delta G''_E$) relative to the woHIU case. In contrast, values for $\Delta G''_E$ were insignificant at 26 °C.

The strain (%) at the crossover point (where $G' = G''$) was determined for each of the HIU power and supercooling treatments (see Fig. S3 (ESI)†). At T_c = 26 °C, the value of strain increases incrementally with increasing HIU power level,

however, this difference only become significant ($p < 0.05$) from the woHIU treatment at the highest power employed (75 W). In contrast, at T_c = 30 °C the crossover strain value remains consistent for increasing HIU power, considering the confidence intervals. As observed at 26 °C, a significantly greater value ($p < 0.05$) was reported for sonication at 75 W relative to the woHIU treatment. This value at 75 W was significantly greater than all other HIU powers ($p < 0.05$). This suggests that samples sonicated at 75 W require a larger strain for the crystalline structure to transition from exhibiting elastic to viscous material characteristics. This transition is more gradual at higher supercooling (ΔT_{SC} = 9 °C) compared to lower supercooling (ΔT_{SC} = 5 °C). Mean values and 95% confidence intervals are summarised in Table S4 (ESI).†

Melting behaviour

The melting profiles of an APS sample crystallised in the absence and the presence of HIU delivered at selected powers between (10–75) W at T_c = 26 °C and 30 °C are given in Fig. S5 (ESI).† Fig. 8A shows the peak melting temperature (T_p) taken from DSC melting profiles compared for the two supercooling temperatures remained similar. At 26 °C, values of T_p were not significantly for all HIU power levels, except 10 W ($p = 0.03$), compared to values for lipid crystallisation without HIU. In addition, significant differences ($p = 0.006$) between peak melting temperatures for samples sonicated at 10 W and 75 W power were identified. For 30 °C, T_p values generally decreased across the ultrasonic power level range. The mean T_p values were significant ($p < 0.001$) for all HIU powers compared to woHIU sample treatment, as indicated (––). Between crystallisation temperatures, values of T_p are significantly different between woHIU at 30 °C and all HIU powers, except 75 W, at 26 °C. The melting enthalpy (ΔH_m) for APS crystallised at 26 °C remained consistent in both the presence and absence of HIU, irrespective of the acoustic powers employed (see Fig. 8B). Samples crystallised without HIU treatment exhibited significantly lower melting enthalpies for lower supercooling (ΔT_{SC} = 5 °C) for sonication at both 51 and 75 W powers ($p < 0.05$). The melting enthalpies were significantly different ($p < 0.05$) between woHIU treatment at T_c = 30 °C and all applied HIU powers, except 75 W, at T_c = 26 °C. The largest effect of HIU power occurs at ΔT_{SC} = 5 °C (T_c = 30 °C) where the values of ΔH_m increase and become like the consistent values measured for 26 °C under all conditions. This could be attributed to the changes in the crystal structure observed under the conditions employed. Here the application of HIU reduces the dissimilarity of the crystalline networks formed under the different supercooling conditions. This is of interest as it indicates a beneficial effect of HIU on these materials.

Cavitation

During all the selected sonication powers, a different cavitation cluster environment is generated. These clusters exhibit a growth-collapse phase that oscillates at different frequencies, relative to the drive frequency (f), depending on the applied acoustic power. Fig. 9 shows a set of hydrophone signals
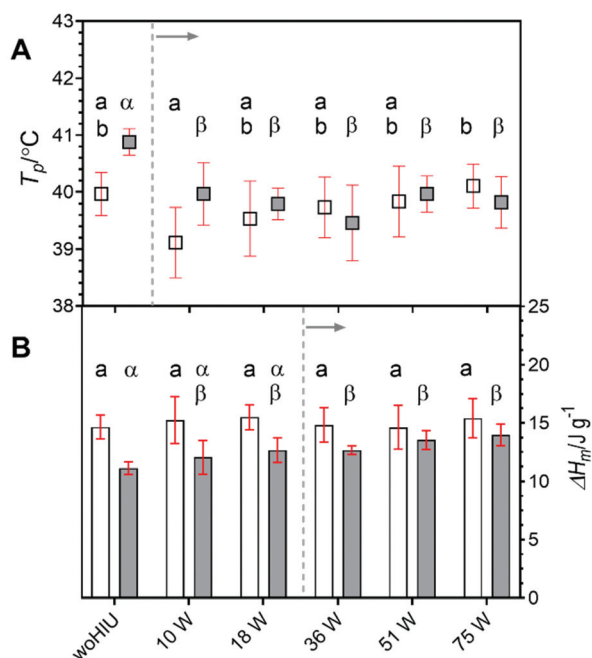
Fig. 8 Plot showing the peak melting temperature (T_p) (A) and melting enthalpy (ΔH_m) (B) of APS crystallised for 60 minutes at 26 °C (☐) and 30 °C (▣) in the presence and absence (woHIU) of high intensity ultrasound applied at power levels of 10 W, 18 W, 36 W, 51 W and 75 W. Both T_p and ΔH_m values become significantly different from the woHIU treatment at 30 °C above HIU power levels as indicated (−−), whereas remain non-significant at 26 °C. Mean values are plotted with 95% confidence levels from six repeat measurements, recorded over three replicate crystallisation experiments.
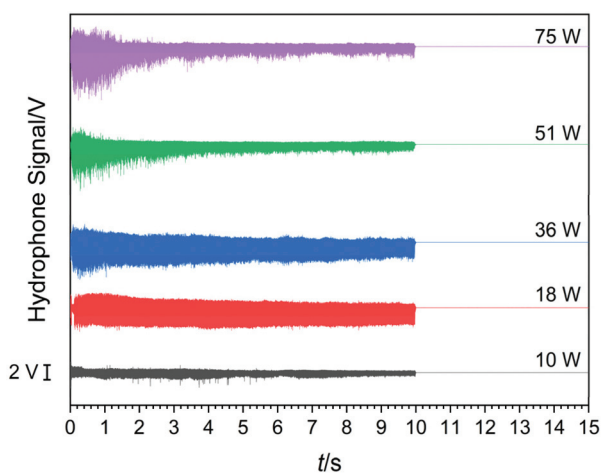

Fig. 9 Plot showing the hydrophone time series collected during HIU treatment in APS (T_c = 26 °C) for 10 s pulse duration and a further 5 s after the cavitation period. HIU powers are indicated by each trace. Scale bar represents 2 V for hydrophone signal for comparison.

recorded as a function of time as HIU was applied at each HIU power level employed for T_c = 26 °C. A total 15 s period was analysed, consisting of a 10 s HIU pulse and a further 5 s section after HIU was terminated. In all cases, no acoustic

emission was observed after HIU source was switched off and had rung down. This indicates that the emission is related to the HIU source, and the cluster generated and that, barring a short ring down period, further cluster collapse does not occur. The lowest acoustic emission was reported at a HIU power of 10 W, in the presence of the bifurcated streamer (BiS) and its alternating bi-cluster (each at frequency = $f/2$) cavitation environment. This unique cavitation cluster remains stable at 10 W but is extremely short-lived at higher HIU powers, which instead 'ring up' to produce a stable single cavitation cluster.[28] The reduced hydrophone signal has been previously attributed to the overlap of the acoustic emission of the two clusters, which operate at 180° in antiphase and the associated bubble environment. For 10 W treatment, a bubble cluster (frequency = $f/3$) is formed in the first 50 ms of sonication with hydrophone signal envelope of approximately 3 V. After this period, the signal amplitude rapidly drops (as the BiS event is generated) and remains reasonably consistent over 10 s HIU pulse. Fig. 9 shows that the maximum hydrophone signal amplitude detected increased as the HIU power levels was raised which in turn altered the cluster type generated. Similar trends within the maximum hydrophone signal amplitude and signal envelope over the 10 s HIU pulse duration were observed at 30 °C as depicted in Fig. S6 (ESI†). At both supercooling temperatures, the hydrophone signal decreased over the 10 s HIU exposure period and that the observed change was more prominent for greater ultrasonic powers. The greatest change in the hydrophone signal envelope (ΔV) was recorded at 75 W ($f/7$ cluster), this was largely within the first 3 seconds of sonication. Attenuation of the acoustic emission detected by the hydrophone is likely to be associated with the generation of a large gas bubble population within the lipid media,[44] combined with the absorption effects exhibited by widespread crystal formation.[19] The attenuation and scattering of sound by particles in solution is a complex topic where particle size and sound frequency play important roles.[45–47] Changes to the physical and acoustic properties of a food material are well documented.[48,49] However, observation of the rapid attenuation during the short HIU treatment of the crystallising oil (as reported here) are less well documented. Here we study the effect on the ultrasonic acoustic signal detected by a hydrophone placed with the crystallising media. To compare the changes observed, the hydrophone data was normalised to the greatest signal voltage for each ultrasonic power and the decay of the hydrophone signal envelope was fitted to a second order model. At this time, the choice of a second order approach was dictated by an empirical need to fit the data to a suitable mathematical form. Further work is needed to develop a more appropriate physical relationship between the absorption vs. time profiles, which is beyond the current scope of the work presented.

Using this assumed model, changes in the hydrophone signal envelope amplitude ([P_A]) with respect to time (t) can be expressed as:

$$\frac{d[P_A]}{dt} = -k[P_A]^2 \tag{2}$$

where k is the apparent rate term describing the attenuation of the hydrophone signal. Integration of this expression with appropriate limits gives:

$$\frac{1}{[P_A]_t} = \frac{1}{[P_A]_0} + kt \qquad (3)$$

where $[P_A]_0$ is the maximum hydrophone signal amplitude considered and $[P_A]_t$ is the amplitude of the hydrophone signal as a function of time. The fit of the data yielded an apparent rate constant ($k/V^{-1} s^{-1}$) associated with this attenuation. These are summarised in Table S3 (ESI).† The fit of this model to the experimental hydrophone data was good, especially for higher ultrasonic powers ($r^2 > 0.90$), as depicted in Fig. 10. At lower HIU power levels (10–18 W), the second order fit was not as good, with a significantly smaller degree of attenuation within the hydrophone signal compared to higher HIU powers. As such the shape of the hydrophone signal decay curve was not comparable for the lowest and highest HIU power level. Values of the effective rate term (k) for each supercooling and HIU treatment are plotted in Fig. 11 for comparison. In general, the value of k increased with increasing HIU power level and were
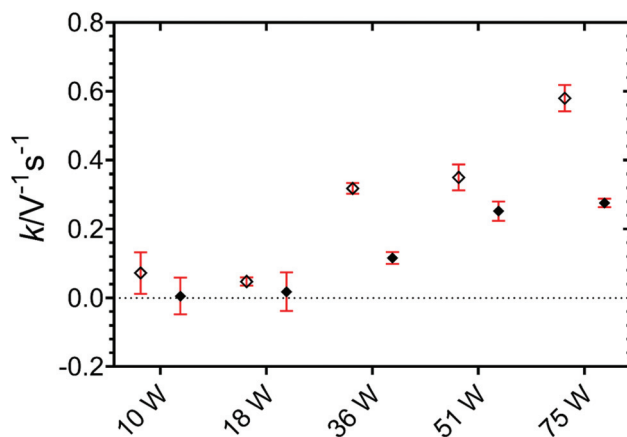

Fig. 11 Plot showing the calculated second order rate constant (k) calculated from fitting of average normalised hydrophone signal to the model as a function of HIU power at crystallisation temperatures of 26 °C (◇) and 30 °C (◆). The 95% confidence interval, calculated from the data fit, is included (in red).

Fig. 10 Plot of the normalised hydrophone signal amplitude with a 100-point moving average applied within the APS sample as a function of time. Here HIU was applied at 10 W (▬), 18 W (▬), 36 W (▬), 51 W (▬) and 75 W (▬) for the entire 10 s period. The sample was recorded at 26 °C (A) and 30 °C (B). Data fit to a second order model (▬) is also shown. Scale bar represents 0.2 V normalised hydrophone signal amplitude. Note the plots are each normalised to the initial value and offset so that each can be viewed in the plot.

greater at ΔT_{SC} = 9 °C compared to ΔT_{SC} = 5 °C. Fig. 11 shows that at ΔT_{SC} = 9 °C (◇) values of k were significantly higher at HIU power levels above 36 W ($p < 0.05$) compared to 10 W and 18 W treatments. HIU applied at 51 W showed no significant difference to the 36 W treatment, but samples sonicated at 75 W had a significantly higher value of k relative to all other powers. Similar trends were observed at ΔT_{SC} = 5 °C (◆), where individual values of k were not significantly different at 10 W, 18 W and 36 W treatments, but all k values were lower than those recorded with sonication at 51 W and 75 W ($p < 0.05$). Finally, there were no significant differences between values from samples treated above 36 W at ΔT_{SC} = 5 °C (◆). The changes in the observed values of k can be attributed to differences within the crystallisation conditions at the two supercooling values employed, highlighted previously within Fig. 2.

Conclusion

The crystallisation behaviour of an APS sample was studied in the presence of HIU at two supercooling conditions. The influence of several ultrasonic powers was investigated, each chosen to generate distinct cavitation cluster regimes. Shorter induction times of crystallisation and faster crystal growth rates were reported for all HIU treatments compared to untreated samples. Changes in the parameters studied appear more significant with increasing ultrasonic power and at lower supercooling (ΔT_{SC} = 5 °C $vs.$ ΔT_{SC} = 9 °C). HIU at only 10 W, which generated a unique bi-cluster (BiS) cavitation regime, exhibited notable changes in crystallisation kinetics comparable to more energy intensive treatments, characterised by a single cavitation cluster. Harder and more elastic lipid samples, comprised of a more closed network of small crystals, were observed with treatment at increasing ultrasonic power. Changes in elasticity compared to non-sonicated samples were
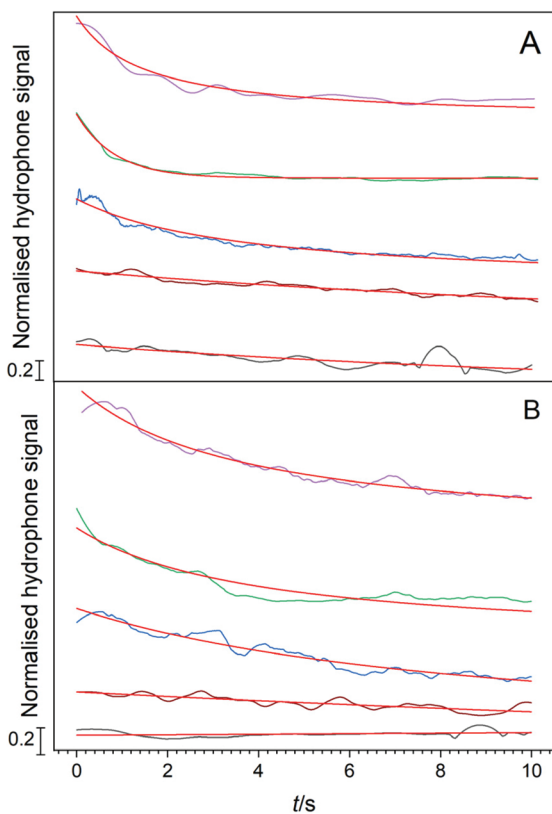
more significant for crystallisation at $\Delta T_{SC} = 9\ °C$, however the hardness was largely independent of supercooling. A decrease in the acoustic emission during the application of HIU was recorded over the 10 s pulse duration and the decay of signal was fitted to an empirical model. Values of the associated rate term increased with increasing HIU power level at both supercooling conditions, which presumably correlated to more rapid signal attenuation and could be associated with increased scattering associated with higher bubble populations and crystal fragmentation.

Conflicts of interest

There are no conflicts to declare.

Acknowledgements

References

1 J. Zhu, H. An, M. Alheshibri, L. Liu, P. M. J. Terpstra, G. Liu and V. S. J. Craig, *Langmuir*, 2016, **32**, 11203–11211.

2 S. Koda and K. Yasuda, in *Sonochemistry and the Acoustic Bubble*, Elsevier Inc., 2015, pp. 151–169.

3 T. Kondo, in *Sonochemistry and the Acoustic Bubble*, Elsevier Inc., 2015, pp. 207–230.

4 T. G. Leighton, *The Acoustic Bubble*, Academic Press, London, 1994.

5 F. R. Young, *Cavitation*, Imperial College Press, London, 1999.

6 K. S. Suslick, D. A. Hammerton and R. E. Cline, *J. Am. Chem. Soc.*, 1986, **108**, 5641–5642.

7 E. B. Flint and K. S. Suslick, *Science*, 1991, **253**, 1397–1399.

8 Acumen Research and Consulting, https://www.acumenresearchandconsulting.com/edible-oil-and-fats-market, (accessed 29/04/2020).

9 K. Higaki, S. Ueno, T. Koyano and K. Sato, *J. Am. Oil Chem. Soc.*, 2001, **78**, 513–518.

10 J. Lee, R. C. da Silva, V. Gibon and S. Martini, *J. Food Sci.*, 2018, **83**, 902–910.

11 A. H. Suzuki, J. Lee, S. G. Padilla, S. Martini, A. H. Suzuki, J. Lee and S. G. Padilla, *J. Food Sci.*, 2010, **75**, E208–E214.

12 Y. Ye, A. Wagh and S. Martini, *J. Agric. Food Chem.*, 2011, **59**, 10712.

13 P. Lawler and P. Dimick, in *Food Lipids: Chemistry, Nutrition, and Biotechnology, Fourth Edition*, ed. C. Akoh, Marcel Dekker, Inc., 2017, pp. 294–319.

14 S. Martini, in *Sonocrystallization of Fats*, Springer International Publishing, New York, 2013, pp. 41–62.

15 FDA, *Fed. Regist.*, 2016, **81**, 54960–55055.

16 R. J. De Souza, A. Mente, A. Maroleanu, A. I. Cozma, V. Ha, T. Kishibe, E. Uleryk, P. Budylowski, H. Schünemann, J. Beyene and S. S. Anand, *Br. Med. J.*, 2015, **351**, 1–16.

17 M. M. Wayland, in *Federal Register*, 2015, vol. 80, pp. 34650–34670.

18 R. Ganguly and G. N. Pierce, *Mol. Nutr. Food Res.*, 2012, **56**, 1090–1096.

19 S. Martini, R. Tejeda-Pichardo, Y. Ye, S. G. Padilla, F. K. Shen and T. Doyle, *J. Am. Oil Chem. Soc.*, 2012, **89**, 1921–1928.

20 R. C. Silva, J. Lee, V. Gibon and S. Martini, *J. Am. Oil Chem. Soc.*, 2017, **94**, 1063–1076.

21 J. M. Maruyama, A. Wagh, L. A. Gioielli, R. C. da Silva and S. Martini, *Food Res. Int.*, 2016, **86**, 54–63.

22 K. Sato, L. Bayés-García, T. Calvet, M. À. Cuevas-Diarte and S. Ueno, *Eur. J. Lipid Sci. Technol.*, 2013, **115**, 1224–1238.

23 S. Martini, J. V. Kadamne, E. A. Ifeduba and C. C. Akoh, *J. Am. Oil Chem. Soc.*, 2017, **94**, 1045–1062.

24 A. Wagh, P. Birkin and S. Martini, in *Annual Review of Food Science and Technology*, ed. T. Doyle and M. P. Klaenhammer, USA, 2016, vol. 7, pp. 23–41.

25 Z. Zhang, D. W. Sun, Z. Zhu and L. Cheng, *Compr. Rev. Food Sci. Food Saf.*, 2015, **14**, 303–316.

26 C. Himawan, V. M. Starov and A. G. F. Stapley, *Adv. Colloid Interface Sci.*, 2006, **122**, 3–33.

27 A. A. Atchley and L. A. Crum, in *Ultrasound: its chemical, physical and biological effects*, ed. K. S. Suslick, 1985, pp. 1–64.

28 P. R. Birkin, T. M. Foley, T. T. Truscott, A. Merritt and S. Martini, *Phys. Chem. Chem. Phys.*, 2017, **19**, 6785–6791.

29 K. B. Bader, J. Mobley, C. C. Church and D. F. Gaitan, *J. Acoust. Soc. Am.*, 2012, **132**, 2286–2291.

30 I. R. Webb, S. J. Payne and C.-C. Coussios, *J. Acoust. Soc. Am.*, 2011, **130**, 3458–3466.

31 P. R. Birkin, J. J. Youngs, T. T. Truscott, S. Martini and T. T. Truscott, *Ultrason. Sonochem.*, 2020, **67**, 1–6.

32 F. Chen, H. Zhang, X. Sun, X. Wang and X. Xu, *J. Am. Oil Chem. Soc.*, 2013, **90**, 941–949.

33 Y. Ye and S. Martini, *J. Agric. Food Chem.*, 2015, **63**, 319–327.

34 M. Patrick, R. Blindt and J. Janssen, *Ultrson. Sonochem.*, 2004, **11**, 251–255.

35 Y. Ye, C. Y. Tan, D. A. Kim and S. Martini, *J. Am. Oil Chem. Soc.*, 2014, **91**, 1155–1169.

36 F. Reuter, S. Lesnik, K. Ayaz-Bustami, G. Brenner and R. Mettin, *Ultrason. Sonochem.*, 2019, **55**, 383–394.

37 P. R. Birkin, H. L. Martin, J. J. Youngs, T. T. Truscott, A. S. Merritt, E. J. Elison and S. Martini, *J. Am. Oil Chem. Soc.*, 2019, **96**, 1197–1204.

38 I. Foubert, K. Dewettinck and P. A. Vanrolleghem, *Trends Food Sci. Technol.*, 2003, **14**, 79–92.

39 W. Kloek, P. Walstra and T. van Vliet, *J. Am. Oil Chem. Soc.*, 2000, **77**, 389–398.

40 K. Sato, *Lipid*, 1999, **101**, 467–474.

41 T. Tran and D. Rousseau, *Food Res. Int.*, 2016, **81**, 157–162.

42 A. Vancleef, S. Seurs, J. Jordens, T. Van Gerven, L. C. J. Thomassen and L. Braeken, *Crystals*, 2018, **8**, 326.

43 S. S. Narine and A. G. Marangoni, *Lebensm. – Wiss. Technol.*, 2001, **34**, 33–40.

44 M. Ichihara, H. Ohkunitani, Y. Ida and M. Kameda, *J. Volcanol. Geotherm. Res.*, 2004, **129**, 37–60.

45 R. J. Urick, *J. Acoust. Soc. Am.*, 1948, **20**, 283–289.

46 S. A. Moore and A. E. Hay, *J. Acoust. Soc. Am.*, 2009, **126**, 1046–1056.

47 D. J. McClements and J. N. Coupland, *Colloids Surf., A*, 1996, **117**, 161–170.

48 R. Saggin and J. N. Coupland, *Food Res. Int.*, 2002, **35**, 999–1005.

49 İ. Gülseren and J. N. Coupland, *Cryst. Growth Des.*, 2007, **7**, 912–918.